Journal of Molecular Modeling (2018) 24: 223
https://doi.org/10.1007/s00894-018-3759-8

ORIGINAL PAPER

Accuracy of auxiliary density functional theory hybrid calculations for activation and reaction enthalpies of pericyclic reactions

José R. Gómez-Pérez[1] · Francisco A. Delesma[2] · Patrizia Calaminici[1,2] · Andreas M. Köster[1,2]

Received: 28 May 2018 / Accepted: 24 July 2018 / Published online: 4 August 2018
© Springer-Verlag GmbH Germany, part of Springer Nature 2018

Abstract

Auxiliary density functional theory (ADFT) hybrid calculations are based on the variational fitting of the Coulomb and Fock potential and, therefore, are free of four-center electron repulsion integrals. So far, ADFT hybrid calculations have been validated successfully for standard enthalpies of formation. In this work the accuracy of ADFT hybrid calculations for the description of pericyclic reactions was quantitatively validated at the B3LYP/6-31G*/GEN-A2* level of theory. Our comparison with conventional Kohn-Sham density functional theory (DFT) results shows that the DFT and ADFT activation and reaction enthalpies are practically indistinguishable. A systematic study of various functionals (PBE, B3LYP, PBE0, CAMB3LYP, CAMPBE0 and HSE06) and basis sets (6-31G*, DZVP-GGA and aug-cc-pVXZ; X = D, T and Q) revealed that the ADFT HSE06/aug-cc-pVTZ/GEN-A2* level of theory yields best balanced accuracy for the activation and reaction enthalpies of the studied pericyclic reactions. With the successfully validate ADFT composite approach consisting of PBE/DZVP-GGA/GEN-A2* structure and transition state optimizations and single-point HSE06/aug-cc-pVTZ/GEN-A2* energy calculations, an accurate, reliable and efficient computational approach for the study of pericyclic reactions in systems at the nanometer scale is proposed.

Keywords Pericyclic reactions · Activation enthalpies · Reaction enthalpies · ADFT · deMon2k

Introduction

Over the last decade, auxiliary density functional theory (ADFT) has been established as a computational efficient alternative to Kohn-Sham density functional theory (DFT) [1, 2]. ADFT is based on the variational fitting of the Coulomb potential as proposed by Dunlap et al. [3–5]. To further increase computational performance, in ADFT the auxiliary density obtained from the variational fitting of the Coulomb potential is also used for the calculation of the exchange-correlation energy and potential [6–9]. As a result, already for small systems, the calculation of the ADFT Kohn-Sham matrix becomes linear, scaling with system size [10] because its elements depend only on the fitting coefficients and not on the density matrix. The simplified structure of the ADFT Kohn-Sham (KS) matrix calculation also permits the development of efficient parallelization algorithms [11]. However, a severe drawback of the ADFT approach so far discussed is represented by its limitation to "pure" density functionals, i.e., functionals that depend only on density and its derivatives. With the recently developed variational fitting of the Fock potential [12], this limitation is lifted. As a result, global [13] and range-separated [14] hybrid functionals can now also been used with ADFT. So far, the performance and accuracy of hybrid functionals within ADFT have been validated extensively for standard enthalpies of formation. The results obtained are in excellent agreement with those from conventional KS-DFT calculations, employing four-center electron repulsion integrals (ERIs) and using the Kohn-Sham density for

This paper belongs to Topical Collection International Conference on Systems and Processes in Physics, Chemistry and Biology (ICSPPCB-2018) in honor of Professor Pratim K. Chattaraj on his sixtieth birthday

Electronic supplementary material The online version of this article (https://doi.org/10.1007/s00894-018-3759-8) contains supplementary material, which is available to authorized users.

✉ Patrizia Calaminici
pcalamin@cinvestav.mx

✉ Andreas M. Köster
akoster@cinvestav.mx

[1] Departamento de Química, CINVESTAV, Centro de Investigación y de Estudios Avanzados, Av. Instituto Politécnico Nacional 2508, A.P. 14-740, 07000 México D.F, Mexico

[2] Programa de Doctorado en Nanociencias y Nanotecnología, CINVESTAV, Instituto Politécnico Nacional 2508, A.P. 14-740, 07000 Ciudad de México, Mexico

the calculation of the exchange-correlation energy and potential. At the same time, the computational performance of ADFT hybrid functional calculations is significantly superior to that of corresponding conventional KS-DFT calculations.

Whereas ADFT hybrid functional calculations of standard enthalpies of formation have been already extensively validated, corresponding validations for activation and reaction enthalpies are less abundant. To the best of our knowledge, attention has so far focused only on reactions contained in the HTBH38/08 and NHTBH38/08 databases [15–17]. For these simple reactions, the activation energies obtained from ADFT hybrid functional calculations compare very favorably with those from conventional four-center ERI KS calculations. These results have encouraged us to investigate the accuracy of ADFT hybrid calculations for the activation and reaction energies of more complex reactions. To this end, we studied a set of hydrocarbon pericyclic reactions proposed by Houk and co-workers for the benchmarking of computational methods [18]. As pointed out by these authors [18], hydrocarbon pericyclic reactions are particularly well suited to the validation of computed classical activation barriers. For completeness, we show schematically in Fig. 1 the reactions considered here. Although our focus is on ADFT B3LYP results, which we can compare directly with their four-center ERI counterparts from the literature, in our ADFT study we also employed various global and range-separated hybrid functionals in combination with several basis sets. Our focus here is on the accuracy and computational performance of the different computational methodologies. We also investigated the accuracy of composite approaches that combine structure and transition state optimizations with the generalized gradient approximation (GGA) with single-point energy calculations employing hybrid functionals. The accuracies in these studies are judged by the comparison of the activation and reaction enthalpies with recommended experimental-theoretical data from the literature [18].

The paper is organized as follows. The next section describes the computational methodology. The ADFT activation and reaction enthalpies for the studied pericyclic reactions are presented in "Results and Discussion" and compared to corresponding four-center ERI KS results and experimental data. The paper finishes with final Conclusions.

Computational methods

All calculations were performed with a development version of the quantum chemistry code deMon2k [19]. For the linear combination of Gaussian type orbital (LCGTO) expansions, Hartree-Fock-optimized 6-31G* [20], DFT-optimized DZVP-GGA [21] and the correlation consistent aug-cc-pVXZ (X = D, T and Q) [22] basis sets were used. The calculation of four-center ERIs was avoided by the variational fitting of the Coulomb and Fock potential. For the expansion of the auxiliary density and orbital product densities the automatically generated GEN-A2* auxiliary function set [21] was used. It contains s, p, d, f and g auxiliary functions that are grouped together into sets with common exponents. The auxiliary density was also used to calculate the exchange-correlation energy and potential, i.e., the ADFT approach was employed. As exchange-correlation functionals, we used PBE [23] as typical example of the generalized gradient approximation, B3LYP

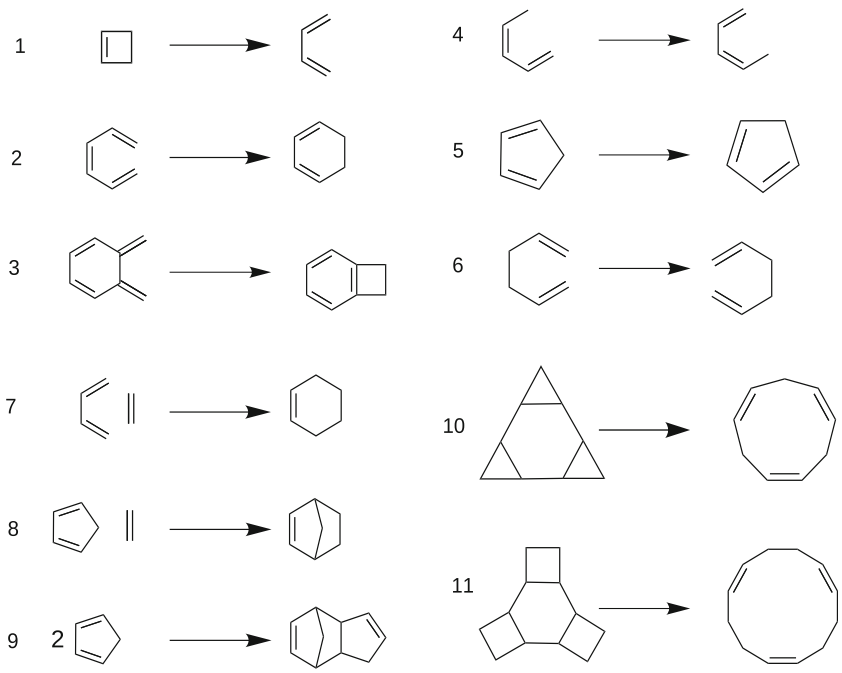

Fig. 1 Reaction schemes of the pericyclic reactions used for auxiliary density functional theory (ADFT) benchmarking

Table 1 Comparison of auxiliary density functional theory (ADFT) B3LYP/6-31G*/GEN-A2* $\Delta H^{\ddagger}_{0K}$ and ΔH^{rxn}_{0K} with corresponding Kohn-Sham (KS) B3LYP/6-31G* results from the literature and experimental data [18]. All values are in kcal mol^{-1}

Reaction	ADFT B3LYP/6-31G*/GEN-A2*		KS B3LYP/6-31G*		Experimental	
	$\Delta H^{\ddagger}_{0K}$	ΔH^{rxn}_{0K}	$\Delta H^{\ddagger}_{0K}$	ΔH^{rxn}_{0K}	$\Delta H^{\ddagger}_{0K}$	ΔH^{rxn}_{0K}
1	34.1	−12.5	33.9	−12.7	31.9	−10.6
2	30.0	−12.9	30.1	−12.5	30.2	−15.3
3	27.1	−14.6	27.3	−14.1	29.1	−10.5
4	36.7	0.0	36.6	0.0	36.7	0.0
5	27.0	0.0	26.6	0.0	23.7	0.0
6	34.0	0.0	34.1	0.0	34.5	0.0
7	24.8	−36.9	24.9	−36.6	23.3	−39.6
8	22.3	−19.0	22.2	−18.6	21.6	−23.2
9	21.1	−11.5	21.1	−11.1	15.1	−19.7

[24] and PBE0 [25] as examples of global hybrid functionals, and CAMB3LYP [26], CAMPBE0 [27] and HSE06 [28] as examples of range-separated hybrid functionals. For all other keywords, the deMon2k default options were used.

All reactant and product structures were fully optimized without symmetry constraints with the B3LYP/6-31G*/GEN-A2* and PBE/DZVP-GGA/GEN-A2* methodologies. The obtained minimum structures were characterized by frequency analyses. For the transition state search, a hierarchically two step procedure [29] was used. First, double-ended saddle interpolations starting with the optimized reactant and product structures were employed in order to find appropriate start structures for the local transition state optimizations. In a second step, the transition states were optimized by an uphill trust region method [30, 31]. For the local quasi-Newton transition state optimizations, the start Hessian matrices were calculated. Once the transition state structures were optimized, they were characterized by frequency analyses. To ensure that the obtained transition states indeed connect the reactants and products initially used in the double-ended saddle interpolation, the intrinsic reaction coordinates (IRCs) were calculated [32]. We note that the approach described here for the optimization of transition states is general, but also applicable to multi-step reactions with non-intuitive transition state structures [33].

For the calculation of activation and reaction enthalpies of the reactions depicted schematically in Fig. 1, the following comments are in order. In reaction **1** butadiene is calculated in trans configuration for the product energy. The reactant in reaction **2** is calculated as cis-hexa-1,3,5-triene. The reactants and products of reaction **4** and **6** are cis-1,3-pentadiene and 1,5-hexadiene, respectively. The reactants for the cycloaddition reactions **7**, **8** and **9** are calculated separately for the corresponding energies. In reaction **7**, butadiene is calculated in trans configuration. For reaction **9**, the endo reaction path is considered.

Results and discussion

Validation of ADFT B3LYP hybrid calculations

To validate ADFT B3LYP activation and reaction enthalpies for pericyclic reactions, we followed the approach of Houk and co-workers [18]. They studied the first nine reactions from Fig. 1 at the B3LYP/6-31G* level of theory with a conventional four-center ERI KS approach and compared the obtained activation, $\Delta H^{\ddagger}_{0K}$, and reaction, ΔH^{rxn}_{0K}, enthalpies with carefully selected experimental data adjusted to 0 K. Reactions **10** and **11** from Fig. 1 were omitted because of the large

Table 2 Mean absolute deviation (MAD) of ADFT activation enthalpies from single-point energy calculations with different density functionals and basis sets employing B3LYP/6-31G*/GEN-A2* optimized reactant, transition state and product structures. All values are in kcal mol^{-1}

Functional Basis	PBE	B3LYP	PBE0	CAMB3LYP	CAMPBE0	HSE06
6-31G*	4.2	2.2	4.1	4.9	7.5	3.5
DZVP-GGA	4.0	2.6	3.5	5.1	7.1	2.7
aug-cc-pVDZ	4.0	2.2	3.3	4.5	6.8	2.7
aug-cc-pVTZ	4.1	3.4	2.8	5.5	6.4	2.7
aug-cc-pVQZ	4.1	3.3	2.7	5.4	6.5	2.7

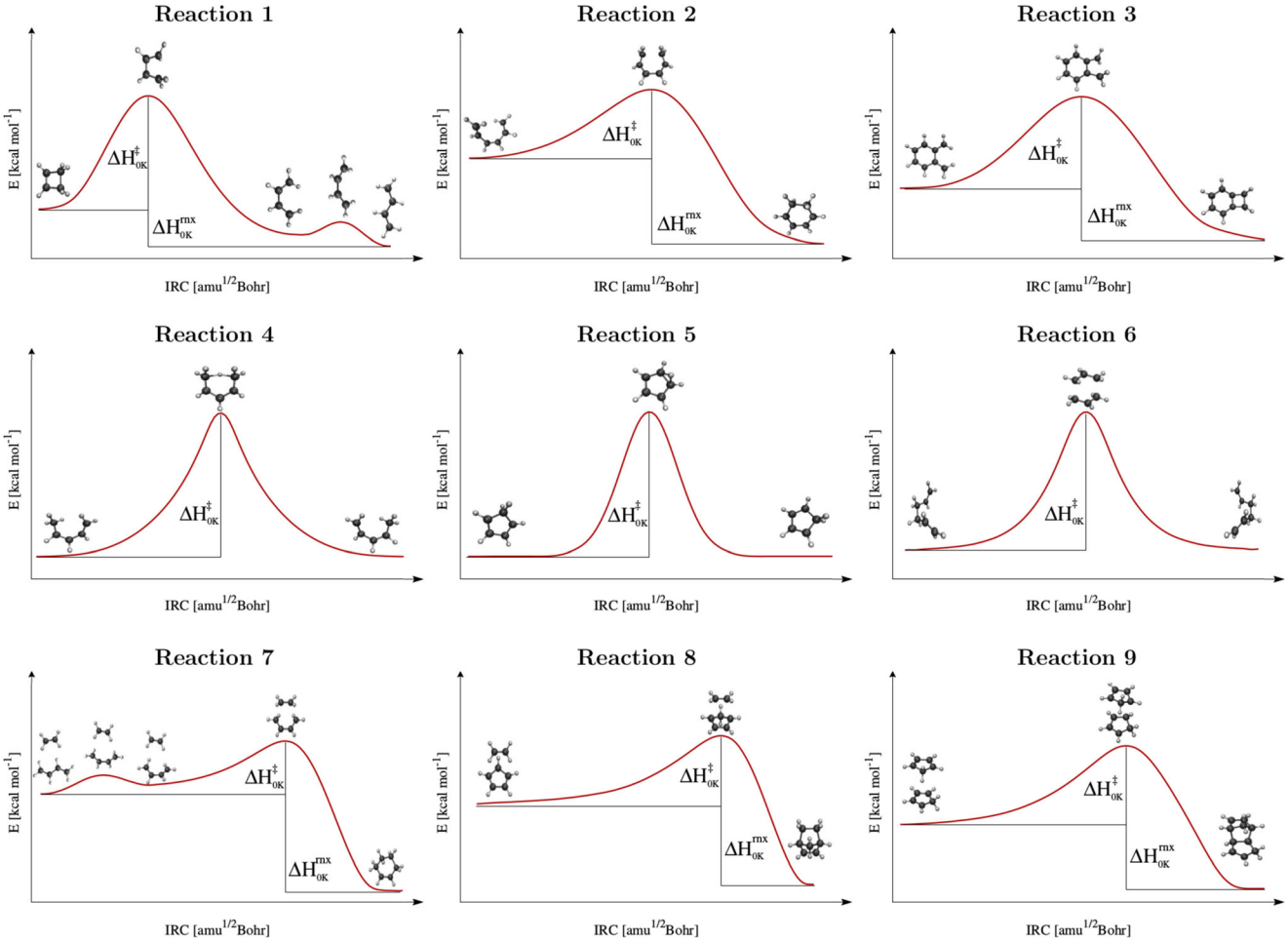

Fig. 2 ADFT B3LYP/6-31G*/GEN-A2* reaction profiles for the first nine pericyclic reactions

uncertainties in the experimental reference data. For the conventional KS B3LYP/6-31G* level of theory, the corresponding ADFT level of theory is B3LYP/6-31G*/GEN-A2*. Therefore, we optimized the reactants, transition states and products at this level of theory employing ADFT. Table 1 compares the ADFT $\Delta H^{\ddagger}_{0K}$ and ΔH^{rxn}_{0K} from this work with those from [18] and the corresponding experimental data. For the zero point energy correction we scaled the ADFT B3LYP/6-31G*/GEN-A2* zero point energies by a factor of 0.9804 according to the literature [18]. As Table 1 shows, the ADFT and conventional KS activation enthalpies differ usually by 0.1 to 0.2 kcal mol^{-1}. The largest deviation of 0.4 kcal mol^{-1} is found for reaction **5**, the [1,5]-sigmatropic shift of hydrogen in cyclopentadiene. For the corresponding reaction enthalpies, slightly larger differences are observed. They are, however, all below or equal to 0.5 kcal mol^{-1}. Taking into account that these results were obtained from two different programs using default settings, the agreement between ADFT and conventional KS activation and reaction enthalpies for the studied pericyclic reactions can be considered quantitative.

For most reactions, the comparison to experimental data was also very satisfying. Notable exceptions are reaction **5** and **9**. For reaction **5**, the [1,5]-sigmatropic shift of hydrogen in cyclopentadiene, the basis set used is not optimal because the hydrogen atom has no polarization functions. Adding p polarization functions to the hydrogen basis, i.e., using the 6-31G** basis, reduces the activation enthalpy from 27.0 to 25.8 kcal mol^{-1}. This value is still above the experimental value (23.7 kcal mol^{-1}) but is now in a similar error range as for other reactions in Table 2. For reaction **9**, we find best agreement with experiment with the PBE functional (PBE/6-31G*/GEN-A2*). The PBE activation and reaction enthalpies are 11.0 kcal mol^{-1} and −18.9 kcal mol^{-1}, respectively. All hybrid functionals deviate significantly from these results. The mean absolute deviation (MAD) for the activation energies, $\Delta H^{\ddagger}_{0K}$, with respect to experiment was reported to be 1.7 kcal mol^{-1} for the conventional KS approach. The corresponding ADFT MAD is 1.8 kcal mol^{-1}. For the six reactions with non-zero reaction enthalpies in Table 1, the MADs from the experimental data are 4.1 kcal mol^{-1} and 3.9 kcal mol^{-1} for the conventional KS approach and for ADFT, respectively.

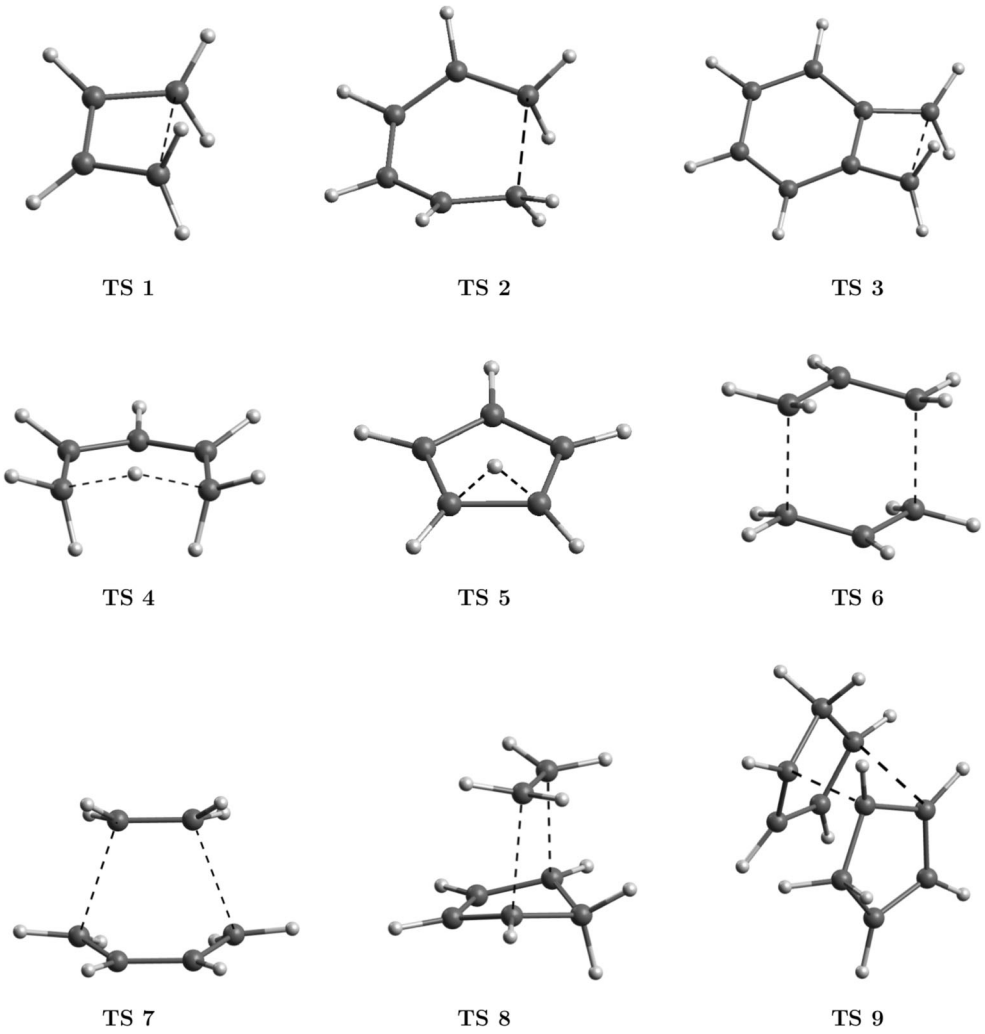

Fig. 3 ADFT B3LYP/6-31G*/GEN-A2* optimized transition state structures for the first nine pericyclic reactions. *Dashed lines* are inserted to guide the eye

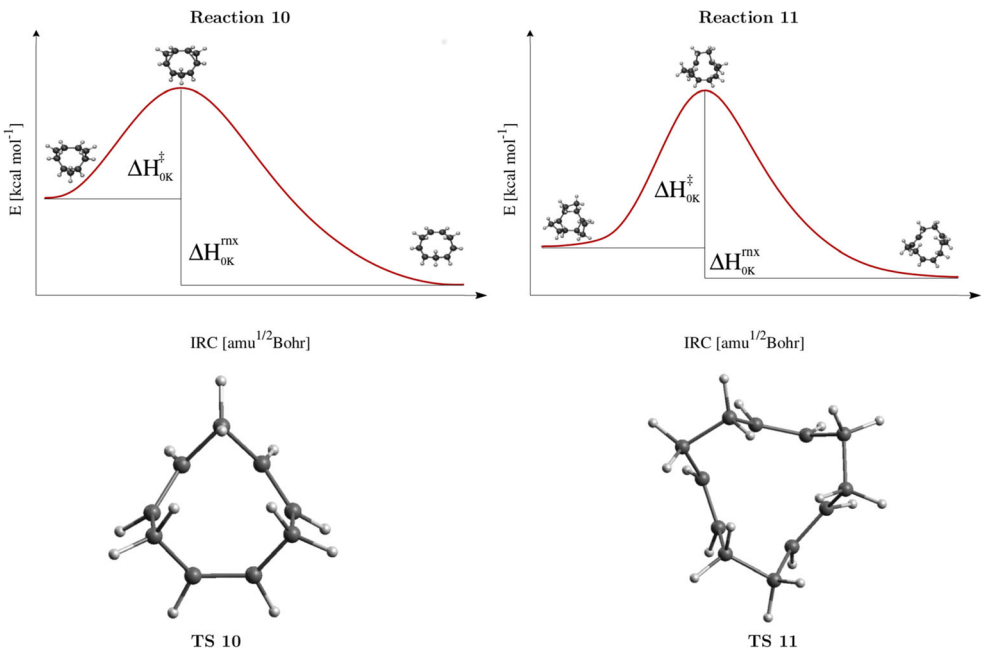

Fig. 4 ADFT B3LYP/6-31G*/GEN-A2* reaction profiles and transition states for reaction 10 and 11

Table 3 MADs of ADFT reaction enthalpies from single-point energy calculations with different density functionals and basis sets employing B3LYP/6-31G*/GEN-A2* optimized reactant, transition state and product structures. All values are in kcal mol^{-1}

Functional Basis	PBE	B3LYP	PBE0	CAMB3LYP	CAMPBE0	HSE06
6-31G*	2.8	3.0	6.0	2.4	15.0	4.1
DZVP-GGA	2.1	4.3	4.4	1.4	13.4	2.7
aug-cc-pVDZ	1.9	4.7	4.1	1.5	12.7	2.6
aug-cc-pVTZ	3.0	7.1	2.5	3.3	10.8	2.4
aug-cc-pVQZ	3.0	7.2	2.3	3.2	10.8	2.6

The ADFT B3LYP/6-31G*/GEN-A2* reaction profiles of the nine pericyclic reactions discussed here are depicted in Fig. 2. Note that for the calculation of these reaction profiles, the reactants in the bimolecular reactions **7**, **8** and **9** are optimized together to form a pre-reaction complex. The calculated IRCs confirm that only reaction **1** and **7** show intermediates according to the cis-trans isomerization of butadiene. These intermediates are directly accessible by the hierarchical two-step transition state search approach employed. The ADFT B3LYP/6-31G*/GEN-A2* optimized transition state structures of the nine pericyclic reactions are depicted in Fig. 3. Their optimized Cartesian coordinates, together with those of the reactants and products, are listed in the Supplementary Information (SI).

Study of functionals and basis sets

After the ADFT B3LYP/6-31G*/GEN-A2* approach had been validated successfully for calculation of pericyclic reactions, we next extended our study to other functionals and basis sets. To this end, we performed single-point energy calculations employing the B3LYP/6-31G*/GEN-A2* optimized reactant, transition state and product structures. We also extended the test set with reaction **10** and **11**. The IRCs and transition state structures for these two reactions are depicted in Fig. 4. As reference for the comparison of our ADFT calculated activation and reaction enthalpies, we used the recommended values from [18].

Tables 2 and 3 report the MADs of the ADFT-calculated activation and reaction enthalpies with respect to the recommended reference values employing the PBE, B3LYP, PBE0, CAMB3LYP, CAMPBE0 and HSE06 functionals in combination with the 6-31G*, DZVP-GGA and aug-cc-pVXZ (X = D, T and Q) basis sets. As can be seen from Table 2, B3LYP/6-31G*/GEN-A2* yields one of the smallest MADs for activation energies. We note that the 2.2 kcal mol^{-1} MAD with ADFT obtained here is in perfect agreement with the corresponding KS MAD found by Houk and co-workers [18]. The good performance of B3LYP/6-31G*/GEN-A2* is due, at least partially, to the used optimized structures from the same level of theory. From the other functionals, only PBE0 and HSE06 reached comparable accuracies for activation energy MADs. The PBE0 activation energy MADs of the pericyclic reactions studied here show a very systematic improvement with basis set size. Convergence is nearly reached with the aug-cc-pVTZ basis with a MAD of 2.8 kcal mol^{-1}. Further increase of the basis set to aug-cc-pVQZ improves the MAD only marginally to 2.7 kcal mol^{-1}. With the HSE06 functional, this MAD is already reached with the DFT optimized DZVP-GGA basis set. On the other hand, the range-separated CAMB3LYP and CAMPBE0 functionals perform rather poorly for the activation energies of the reactions studied here.

Table 3 lists the MADs for the reaction enthalpies of the 11 studied reactions. Surprisingly, B3LYP/6-31G*/GEN-A2* does not perform best for the reaction enthalpies despite the fact that the structures were optimized at this level of theory. Even more disturbing is the fact that the ADFT B3LYP reaction enthalpies deteriorate significantly with increasing basis set size. We note that this observation is in qualitative agreement with results from Houk and co-workers employing conventional KS methodology. A similar trend can also be seen for the activation energies in Table 2, albeit much less

Table 4 MADs of ADFT activation enthalpies from single-point energy calculations with different density functionals and basis sets employing PBE/DZVP-GGA/GEN-A2* optimized reactant, transition state and product structures. All values are in kcal mol^{-1}

Functional Basis	PBE	B3LYP	PBE0	CAMB3LYP	CAMPBE0	HSE06
6-31G*	4.4	2.2	4.4	5.0	7.8	3.7
DZVP-GGA	4.1	2.5	3.7	4.9	7.3	2.9
aug-cc-pVDZ	4.0	2.1	3.6	4.4	7.1	2.9
aug-cc-pVTZ	3.9	3.0	3.0	5.2	6.8	2.6
aug-cc-pVQZ	4.0	2.9	3.0	5.2	6.8	2.7

Table 5 MADs of ADFT reaction enthalpies from single-point energy calculations with different density functionals and basis sets employing PBE/DZVP-GGA/GEN-A2* optimized reactant, transition state and product structures. All values are in kcal mol^{-1}

Functional Basis	PBE	B3LYP	PBE0	CAMB3LYP	CAM-PBE0	HSE06
6-31G*	2.9	2.7	6.4	2.9	15.7	4.4
DZVP-GGA	2.1	4.2	4.6	1.4	13.9	2.9
aug-cc-pVDZ	1.9	4.5	4.2	1.3	13.1	2.7
aug-cc-pVTZ	2.8	6.7	2.8	2.8	11.5	2.2
aug-cc-pVQZ	2.8	6.7	2.7	2.7	11.6	2.2

pronounced. On the other hand, PBE0 and HSE06 show systematic improvements in the reaction energy MADs with increasing basis set quality. As for the activation energies near basis set convergence is reached for PBE0 and HSE06 with the aug-cc-pVTZ basis with MADs of 2.5 kcal mol^{-1} and 2.4 kcal mol^{-1}, respectively. In view of the rather disappointing performance of range-separated Coulomb-attenuating method (CAM) hybrid functionals for activation energies it is surprising that CAMB3LYP performs best for the reaction energies of the 11 pericyclic reactions with a MAD of 1.4 kcal mol^{-1} employing the CAMB3LYP/DZVP-GGA/GEN-A2* level of theory. Altogether, this study suggests that the ADFT approaches PBE0/aug-cc-pVXZ/GEN-A2* (X = T and Q) and HSE06/aug-cc-pVTZ/GEN-A2* are best suited for the overall description of the studied pericyclic reactions.

To investigate the effect of structure optimization on the MADs for the activation and reaction enthalpies of the studied pericyclic reactions, we have also optimized all structures at the HSE06/aug-cc-pVTZ/GEN-A2* level of theory. In this approach, the MAD of the activation energy reduces by 0.4 kcal mol^{-1} to 2.3 kcal mol^{-1}, and the MAD of the reaction enthalpy remains the same. Thus, HSE06/aug-cc-pVTZ/GEN-A2* outperforms B3LYP/6-31G*/GEN-A2* in terms of accuracy. In this context it is worth mentioning that larger basis sets in hybrid ADFT calculations are much less problematic than in conventional hybrid KS calculations because the N^4scaling, N being the number of basis functions, with respect to the basis set size, is avoided.

Our previous analysis clearly demonstrated that hybrid functionals, here HSE06, are most appropriate for the reliable calculation of activation and reaction enthalpies. On the other hand, it is well know that GGA optimized structure parameters are usually in good agreement with experimental data. Therefore, we also investigated single-point energy calculations with the functionals studied here and basis sets employing ADFT PBE/DZVP-GGA/GEN-A2* optimized reactants, transition states and products. For the zero point energy corrections the unscaled ADFT PBE/DZVP-GGA/GEN-A2* zero point energies were employed. The optimized Cartesian coordinates are listed in the SI. The ADFT PBE/DZVP-GGA/GEN-A2* approach is well suited to the optimization of large molecules on the nanometer length scale where structure optimization with ADFT hybrid functionals will become prohibitively time consuming due to their currently less optimal parallel scaling [14]. Tables 4 and 5 list the MADs of the ADFT-calculated activation and reaction enthalpies with respect to the recommended reference values employing now PBE/DZVP-GGA/GEN-A2* optimized structures. For the activation energies, B3LYP again performs best, either with the 6-31G* or aug-cc-pVDZ basis set. As comparison of Table 4 with Table 2 shows, the change in the structure optimization method has only little effect on the MADs for the activation enthalpies. The same is also true for the corresponding reaction enthalpy MADs as comparison of Table 5 with Table 3 reveals. This finding is also supported by the quantitative comparison of the optimized B3LYP/6-31G*/GEN-A2* and PBE/DZVP-GGA/GEN-A2* structures with a mapping algorithm [34]. The similarity indices obtained, defined on an interval [0, 1] with 1 indicating perfect structure matches, are usually larger than 0.99. Thus, an ADFT composite method consisting of GGA structure optimization (here: PBE/DZVP-GGA/GEN-A2*) and hybrid single-point energy calculations (here: HSE06/aug-cc-pVTZ/GEN-A2*) yields activation and reaction enthalpies for pericyclic reactions that are indistinguishable from a pure hybrid approach. Based on the documented computational performance of ADFT GGA optimization and frequency analysis calculations [35] and ADFT hybrid single-point energy calculations [13, 14] it is foreseeable that the composite method proposed here will permit accurate and reliable calculations of pericyclic reactions involving nanometric systems in very reasonable times. Typical examples are the functionalization of fullerenes and endohedral metal fullerenes by pericyclic reactions [36].

Conclusions

The validation of ADFT B3LYP hybrid calculations for calculation of activation and reaction enthalpies of pericyclic reactions yields quantitative agreement with corresponding conventional KS calculations. A systematic study of functionals and basis sets shows that B3LYP/6-31G*/GEN-A2*

activation energies have the smallest MAD of all functionals but that the corresponding reaction enthalpies are less good. This, in combination with the deterioration of both activation and reaction enthalpies with increasing basis set quality, questions the overall reliability of the B3LYP functional for the study of pericyclic reactions. As an alternative the range-separated HSE06 functional in combination with the aug-cc-pVTZ basis set might be considered. This approach shows MADs in activation and reaction enthalpies that are more balanced as for B3LYP. Moreover, both enthalpies improve systematically with improving basis set quality. For pericyclic reactions involving nanometric systems, a composite approach in which structure optimization at the PBE/DZVP-GGA/GEN-A2* level of theory is combined with single-point energy calculations at the HSE06/aug-cc-pVTZ/GEN-A2* level of theory is suggested. The accuracy of this composite approach is very similar to that of pure hybrid functionals. In combination with the extraordinary computational efficiency of ADFT it will allow accurate and reliable pericyclic reaction studies of systems on the nanometer scale.

Acknowledgments JRGP and FAD gratefully acknowledge funding as a Sistema Nacional de Investigadores (SNI) assistant (15228) and Consejo Nacional de Ciencia y Tecnología (CONACyT) PhD fellow (421457), respectively. This work was financially supported by the CONACyT Project CB-252658 and by the infrastructure Project GIC-268251. The authors are also thankful to Q.I. Luis Lopez-Sosa for valuable discussions.

References

1. Hohenberg P, Kohn W (1964) Inhomogeneous electron gas. Phys Rev 136:B864–B871
2. Kohn W, Sham LJ (1965) Self-consistent equations including exchange and correlation effects. Phys Rev 140:A1133–A1138
3. Dunlap BI, Connolly JWD, Sabin JR (1979) On first-row diatomic molecules and local density models. J Chem Phys 71:4993–4999
4. Mintmire JW, Dunlap BI (1982) Fitting the Coulomb potential variationally in linear-combination-of-atomic-orbitals density-functional calculations. Phys Rev A 25:88–95
5. Mintmire JW, Sabin JR, Trickey SB (1982) Local-density-functional method in two-dimensionally periodic systems. Hydrogen and berillium monolayers. Phys Rev B 26:1743–1753
6. Laikov DN (1997) Fast evaluation of density functional exchange-correlation terms using the expansion of the electron density in auxiliary basis sets. Chem Phys Lett 281:151–156
7. Köster AM, Reveles JU, del Campo JM (2004) Calculation of exchange-correlation potentials with auxiliary function densities. J Chem Phys 121:3417–3424
8. Birkenheuer U, Gordienko AB, Nasluzov VA, Fuchs-Rohr MK, Rösch N (2005) Model density approach to the Kohn–Sham problem: Efficient extension of the density fitting technique. Int J Quantum Chem 102:743–761
9. Bienvenu AV, Knizia G (2018) Efficient treatment of local meta-generalized gradient density functionals via auxiliary density expansion: the density fitting (DF) J + X approximation. J Chem Theory Comput 14:1297–1303
10. Köster AM, Goursot A, Salahub DR (2003) In: McCleverty J, Meyer TJ, Lever B (eds) Comprehensive coordination chemistry II: From biology to nanotechnology, vol 2, Chapter 2.57. Elsevier, Amsterdam, pp 681–685
11. Geudtner G, Janetzko F, Köster AM, Vela A, Calaminici P (2006) Parallelization of the deMon2k code. J Comp Chem 27:483–490
12. Mejía-Rodriguez D, Köster AM (2014) Robust and efficient variational fitting of Fock exchange. J Chem Phys 141:124114
13. Mejía-Rodriguez D, Huang X, del Campo JM, Köster AM (2015) Hybrid functionals with variationally fitted exact exchange. Advances in quantum chemistry, vol 71. Academic, New York
14. Delesma FA, Geudtner G, Mejía-Rodríguez D, Calaminici P, Köster AM (2018) Range-separated hybrid functionals with variational fitted exact exchange. J Chem Theory Comput (submitted)
15. Zhao Y, González-García N, Truhlar DG (2005) Benchmark database of barrier heights for heavy atom transfer, nucleophilic substitution, association, and unimolecular reactions and its use to test theoretical methods. J Phys Chem A 109:2012–2018
16. Zhao Y, Lynch BJ, Truhlar DG (2005) Multi-coefficient extrapolated density functional theory for thermochemistry and thermochemical kinetics. Phys Chem Chem Phys 7:43–52
17. Zhao Y, Schultz NE, Truhlar DG (2006) Design of density functionals by combining the method of constraint satisfaction with parametrization for thermochemistry, thermochemical kinetics, and noncovalent interactions. J Chem Theory Comput 2:364–382
18. Guner V, Khuong KS, Leach AG, Lee PS, Bartberger MD, Houk KN (2003) A standard set of pericyclic reactions of hydrocarbons for the benchmarking of computational methods: the performance of ab initio, density functional, CASSCF, CASPT2, and CBS-QB3 methods for the prediction of activation barriers, reaction energetics, and transition state geometries. J Phys Chem A 107:11445–11459
19. Köster AM, Geudtner G, Álvarez-Ibarra A, Calaminici P, Casida ME, Carmona-Espíndola J, Domínguez VD, Flores-Moreno R, Gamboa GU, Goursot A, Heine T, Ipatov A, de la Lande A, Janetzko F, del Campo JM, Mejía-Rodríguez D, Reveles JU, Vásquez-Pérez J, Vela A, Zuñiga-Gutiérrez B, and Salahub DR (2018) deMon2k Version 5.0. the deMon developers, Cinvestav, Mexico City. See also: www.demon-software.com
20. Hariharan PC, Pople JA (1973) The influence of polarization functions on molecular orbital hydrogenation energies. Theor Chim Acta 28:213–222
21. Calaminici P, Janetzko F, Köster AM, Mejia-Olvera R, Zuniga-Gutierrez B (2007) DFT optimized basis sets for gradient corrected functionals: 3d transition metal systems. J Chem Phys 126:044108
22. Dunning Jr TH (1989) Gaussian basis sets for use in correlated molecular calculations. I. The atoms boron through neon and hydrogen. J Chem Phys 90:1007–1023
23. Perdew JP, Burke K, Ernzerhof M (1996) Generalized gradient approximation made simple. Phys Rev Lett 77:3865–3868
24. Becke AD (1993) Density functional thermochemistry. III. The role of exact exchange. J Chem Phys 98:5648–5652
25. Adamo C, Barone V (1999) Toward reliable density functional methods without adjustable parameters: the PBE0 model. J Chem Phys 110:6158–6170
26. Yanai TDP, Handy NC (2004) A new hybrid exchange–correlation functional using the Coulomb-attenuating method (CAM-B3LYP). Chem Phys Lett 393:51–57
27. Lange AW, Rohrdanz MA, Herbert JM (2008) Charge-transfer excited states in a π-stacked adenine dimer, as predicted using long-range-corrected time-dependent density functional theory. J Phys Chem B 112:6304–6308
28. Krukau AV, Vydrov OA, Izmaylov AF, Scuseria GE (2006) Influence of the exchange screening parameter on the performance of screened hybrid functionals. J Chem Phys 125:224106
29. del Campo JM, Köster AM (2008) A hierarchical transition state search algorithm. J Chem Phys 129:024107

30. Bofill JM (1994) Updated Hessian matrix and the restricted step method for locating transition structures. J Comp Chem 15:1–11
31. Culot P, Dive G, Nguyen VH, Ghuysen JM (1992) A quasi-Newton algorithm for first-order saddle-point location. Theor Chim Acta 82: 189–205
32. Fukui K (1981) The path of chemical reactions—the IRC approach. Acc Chem Res 14:363–368
33. Cruz-Olvera D, de la Trinidad VA, Geudtner G, Vásquez-Pérez JM, Calaminici P, Köster AM (2015) Transition State searches in metal clusters by first principle methods. J Phys Chem A 119:1494–1501
34. Vásquez-Pérez JM, Gamboa GU, Köster AM, Calaminici P (2009) The discovery of unexpected isomers in sodium heptamers by Born-Oppenheimer molecular dynamics. J Chem Phys 131:124126
35. Delgado-Venegas RI, Mejía-Rodríguez D, Flores-Moreno R, Calaminici P, Koster AM (2016) Analytic second derivatives from auxiliary density perturbation theory. J Chem Phys 145:224103
36. Chen M, Lu X, MRM I, Echegoyen L (2015) Endohedral fullerenes in endohedral metallofullerenes: basics and applications. CRC, Boca Raton